

Flavor symmetry breaking and scaling for improved staggered actions in quenched QCD

M. Cheng^a, N. Christ^a, C. Jung^b, F. Karsch^{b,d}, R. Mawhinney^a, P. Petreczky^{b,c}, K. Petrov^e

^a*Physics Department, Columbia University, New York, NY 10027*

^b*Physics Department, Brookhaven National Laboratory, Upton, NY 11973*

^c*RIKEN-BNL Research Center, Brookhaven National Laboratory, Upton, NY 11973*

^d*Fakultät für Physik, Universität Bielefeld, D-33615 Bielefeld, Germany*

^e*Niels Bohr Institute, University of Copenhagen, Blegdamsvej 17, DK-2100 Copenhagen, Denmark*

(November 22, 2018)

Abstract

We present a study of the flavor symmetry breaking in the pion spectrum for various improved staggered fermion actions. To study the effects of link fattening and tadpole improvement, we use three different variants of the p4 action - p4fat3, p4fat7, and p4fat7tad. These are compared to Asqtad and also to naive staggered. To study the pattern of symmetry breaking, we measure all 15 meson masses in the 4-flavor staggered theory. The measurements are done on a quenched gauge background, generated using a one-loop improved Symanzik action with $\beta = 10/g^2 = 7.40, 7.75, \text{ and } 8.00$, corresponding to lattice spacings of approximately $a = .31 \text{ fm.}, .21 \text{ fm.}, \text{ and } .14 \text{ fm.}$ We also study how the lattice scale set by the ρ mass on each of these ensembles compares to one set by the static quark potential.

11.15.Ha, 11.30.Rd, 12.38.Aw, 12.38.-t 12.38.Gc

I. INTRODUCTION

Lattice QCD is the only first-principles technique to calculate various important quantities where the strong nuclear force is an important effect. However, the discretization of QCD on a lattice is plagued by many difficulties. Among them is the existence of doubler modes, which turns one flavor of quark in the continuum limit into 16 flavors on a lattice. Several different methods have been used to eliminate these doubler modes.

One such method was introduced by Kogut and Susskind and involves a thinning of the fermion degrees of freedom by “staggering” the components of the Dirac spinor over a four-dimensional hypercube. While this only reduces the number of doublers from 16 to 4, staggered fermions are useful in that a remnant $U(1)$ chiral symmetry is preserved.

However, staggered fermions mix the spin and flavor degrees of freedom, breaking flavor symmetry. As a result, of the 15 pions in the 4 flavor staggered theory, only the lightest pion is a true Goldstone boson, tending to $m_\pi \rightarrow 0$ as $m_q \rightarrow 0$. The other fourteen pions have their masses increased by $O(a^2)$ terms in the lattice action that do not preserve flavor symmetry. These mass splittings fall into a pattern that reflects the remnant chiral symmetry on the lattice.

Several attempts have been made to improve the staggered fermion action, either by adding new terms to the fermion action (Naik [1], p4 [2]) or by using some variant of gauge-link smearing [3] [4]. In this work, we examine how well some of these improvements do in reducing flavor-symmetry breaking by calculating the masses of all 15 pions in the staggered theory on a quenched background. The flavor symmetry of the pion spectrum has been previously examined on quenched lattices with the naive staggered action [5] and on dynamical lattices with the Asqtad action [6].

The study of flavor symmetry breaking is especially important for simulations of finite-temperature QCD, where chiral symmetry and the dynamics of the the lightest mesons play a crucial role in determining the universal properties of the QCD phase transition. Different variants of the staggered fermion action are used in finite-temperatures simulations because they are numerically inexpensive and naturally allow for $O(a^2)$ improvement through the addition of a Naik or p4 term [7] [8]. Since finite-temperature simulations are currently only feasible for rather small temporal extents ($N_\tau = 4, 6, 8$), and thus very coarse lattices, flavor symmetry improvement is vital for this purpose.

In addition, we examine the scaling properties of these actions by comparing the lattice scales determined by m_ρ to that set by the static quark potential (r_1). Typically, for the naive staggered action, the ratio of the scales set by m_ρ and r_1 depends strongly on the lattice spacing, but studies [9] have shown that the Asqtad action has much better scaling properties than naive the staggered action. Here we test the scaling properties of the various p4 actions described above.

II. ACTIONS

A. Staggered Action

The Kogut-Susskind action is written as:

$$S_F = \sum_x \sum_\mu \eta_\mu(x) \left[\bar{\chi}(x) (U_\mu(x) \chi(x + \mu) - U_\mu^\dagger(x - \mu) \chi(x - \mu)) \right] + 2m \sum_x \bar{\chi}(x) \chi(x) \quad (1)$$

where $\chi(x)$ is a one-component spinors and $\eta_\mu(x) = (-1)^{x_0 + \dots + x_{\mu-1}}$ are the staggered phases.

By distributing the spinor degrees of freedom over a hypercube, the spin and flavor degrees of freedom are mixed by $O(a^2)$ terms in the action. As outlined by Golterman and Smit [10], there are multiple meson states on the lattice that correspond to distinct physical states. For example, there are 15 different operators, falling into 7 distinct irreducible representations that have the quantum numbers of a physical pion.

Because only a $U(1)$ remanant of the continuum chiral symmetry group is preserved, only one of these 15 pions is a true Goldstone boson. The other 14 have masses have non-vanishing masses that are determined by the $O(a^2)$ terms in the action.

B. Improved Staggered Actions

There have been several variants of staggered fermions that seek to improve upon the naive staggered formulation. Two notable examples that are the p4 [2] and Asqtad [3] actions. Both of these actions incorporate an additional three-link term in the fermion derivative. The p4 action includes a bent “knight’s move” term, while Asqtad uses the straight Naik term [1]. These two terms are the minimal allowed modifications of the fermion derivative consistent with the symmetries of the staggered formulation.

A general action with both the Naik and the knight’s move term is written as:

$$\begin{aligned} S_F = & 2m \sum_x \bar{\chi}(x) \chi(x) + \sum_x \bar{\chi}(x) \sum_\mu \eta_\mu(x) \\ & \left\{ c_{1,0} \left[U_\mu(x) \chi(x + \mu) - U_\mu^\dagger(x - \mu) \chi(x - \mu) \right] + \right. \\ & + c_{3,0} \left[U_\mu^{(3,0)}(x) \chi(x + 3\mu) - U_\mu^{(3,0)\dagger}(x - 3\mu) \chi(x - 3\mu) \right] + \\ & + c_{1,2} \sum_{\nu \neq \mu} \left[U_{\mu,\nu}^{(1,2)}(x) \chi(x + \mu + 2\nu) - U_{\mu,\nu}^{(1,2)\dagger}(x - \mu - 2\nu) \chi(x - \mu - 2\nu) + \right. \\ & \left. \left. + U_{\mu,\nu}^{(1,-2)}(x) \chi(x + \mu - 2\nu) - U_{\mu,\nu}^{(1,-2)\dagger}(x - \mu + 2\nu) \chi(x - \mu - 2\nu) \right] \right\} \end{aligned} \quad (2)$$

where

$$\begin{aligned} U_\mu^{(3,0)}(x) &= U_\mu(x) U_\mu(x + \mu) U_\mu(x + 2\mu) \\ U_{\mu,\nu}^{(1,2)}(x) &= \frac{1}{2} \left[U_\mu(x) U_\nu(x + \mu) U_\nu(x + \mu + \nu) + U_\nu(x) U_\nu(x + \nu) U_\mu(x + 2\nu) \right] \\ U_{\mu,\nu}^{(1,-2)}(x) &= \frac{1}{2} \left[U_\mu(x) U_\nu^\dagger(x + \mu - \nu) U_\nu^\dagger(x + \mu - 2\nu) + U_\nu^\dagger(x - \nu) U_\nu^\dagger(x - 2\nu) U_\mu(x - 2\nu) \right] \end{aligned} \quad (3)$$

For the p4 action, $c_{1,2} = 1/24$, $c_{3,0} = 0$; the Naik action has $c_{1,2} = 0$, $c_{3,0} = -1/48$. In the free-field limit, the Naik action eliminates the $O(a^2)$ errors in the quark propagator. The p4 action is chosen to remove the violations to rotational symmetry in the quark propagator through $O(p^4)$.

C. Gauge Link Smearing

It has been shown that gauge link smearing helps reduce the amount of flavor symmetry violation in the fermion action [3]. Gauge link smearing involves replacing the one-link term in the fermion action with some linear combination of gauge invariant staples that connect nearest-neighbor sites.

$$c_1 \longrightarrow + c_3 \Sigma \left[\begin{array}{c} \longrightarrow \\ \longrightarrow \\ \downarrow \end{array} \right] + c_5 \Sigma \left[\begin{array}{c} \longrightarrow \\ \nearrow \\ \downarrow \\ \searrow \end{array} \right] + c_7 \Sigma \left[\begin{array}{c} \longrightarrow \\ \nearrow \\ \downarrow \\ \searrow \\ \nearrow \end{array} \right] \quad (4)$$

The p4fat3 action has been used previously in thermodynamic simulations [11]. Only the three-link staple is included for p4fat3. The smearing coefficients for the Asqtad action are chosen to cancel out the tree-level violations of flavor symmetry. The Asqtad action is also tadpole-improved, and includes the planar, 5-link Lepage term to cancel out the $O(a^2)$ errors introduced by the smearing procedure [3]. The smearing coefficients for p4fat7 and p4fat7tad are determined in the same manner as in Asqtad, but the Lepage term is omitted. In addition, we compare the tadpole-improved p4fat7tad action with the p4fat7 action in order to test the effects of tadpole improvement. A full summary of the smearing parameters can be found in Table I.

III. SIMULATION

A. Gauge Action

To test the properties of the various actions, we measure the meson spectrum on quenched gauge backgrounds with $\beta = 10/g^2 = 7.40, 7.75, 8.00$ using a one-loop improved Symanzik action. For each value of β , we generated 100 configurations. For $\beta = 7.40, 7.75$, we used a volume of $16^3 \times 32$ and separated configurations by 1000 sweeps of the gauge heat bath algorithm. For the finest ensemble, $\beta = 8.00$, we separated configurations by 500 sweeps, on a volume of $24^3 \times 32$. These gauge configurations match those used previously to test the scaling behavior of the Asqtad action [9].

B. Sources

Following Ref. [5], we calculate the quark propagator for eight different wall sources on each configuration by solving using the standard conjugate gradient technique.

$$\sum_{x'} (DD^\dagger)(x, x') X^{\vec{A}}(x') = \sum_{2\vec{y}} \delta_{\vec{x}, 2\vec{y} + \vec{A}} \delta_{x_4, 0} \quad (5)$$

$$\chi^{\vec{A}}(x) = \sum_{x'} D^\dagger(x, x') X^{\vec{A}}(x') \quad (6)$$

where the summation over $2\vec{y}$ goes over all the unit cubes at time slice $t = 0$ and \vec{A} labels each of the eight different corners of a 3-D unit cube. We combine the quark propagators that we obtain into meson propagators:

$$M_{\vec{A}, \vec{B}} = \sum_x D_{\vec{A}} \bar{\chi}^{\vec{A}}(x) D_{\vec{B}} \chi^{\vec{B}}(x) \quad (7)$$

$$D_{\vec{A}} \chi(x) = \sum_{\delta_1 = \pm 1} \sum_{\delta_2 = \pm 1} \sum_{\delta_3 = \pm 1} \chi(x + \delta_1 A_1 \mathbf{e}_1 + \delta_2 A_2 \mathbf{e}_2 + \delta_3 A_3 \mathbf{e}_3) \quad (8)$$

The 64 different meson operators fall into irreducible representations that can be written as linear combinations of the meson propagators defined above using the symmetric shift operator $D_{\vec{A}}$.

$$M(t) = \sum_{\vec{A}} \phi(\vec{A}) M_{\vec{A}, (\vec{A} + \vec{\delta})} \quad (9)$$

$\vec{\delta}$ and $\phi(\vec{A})$ are specified for each irreducible representation. Table II lists the details for all the meson representations. For us, only the meson operators that correspond to a physical pion are of interest. Henceforth, we shall label the meson states using the conventions set forth in [5], which labels meson states by their transformation properties under the lattice symmetry group ($\mathbf{r}^{\sigma_s \sigma_{123}}$).

C. Measurements

For each set of configurations, we measured the 15 different π propagators for at least three different values of m_q . These values are chosen so that m_π falls into approximately the same range for the different actions. By using three masses, we can extrapolate to the $m_q \rightarrow 0$ limit. Values of m_π were then extracted by fitting to the form:

$$M(t) = A \left(e^{-m_+ t} + e^{-m_+(T-t)} \right) + B (-1)^t \left(e^{-m_- t} + e^{-m_-(T-t)} \right) \quad (10)$$

where m_+ and m_- denote the masses of opposite parity states.

For $\beta = 8.00$, we use a fitting range of 6 – 16; for $\beta = 7.75$, we use a range of 5 – 16; and for $\beta = 8.00$, we use 4 – 16 except for staggered fermions, where the larger masses requires us to use a fitting range of 3 – 16 to obtain a good signal.

Tables III-VII show the values for m_π that we have obtained. While we measure masses for all 15 operators, several of the operators are related by lattice symmetries and fall into degenerate triplets. Our data confirms this expected degeneracy, so we have quoted only one value for each of these triplets by averaging together the propagators for each of the operators. As a result, we are left with 7 distinct masses for each set of measurements.

The errors are calculated by using the jackknife method with a block size of one configuration. While we only quote statistical errors, there is an additional systematic error associated with varying the fit range. For most of the measurements, this effect is smaller than the quoted statistical error. However, for the coarsest lattices at $\beta = 7.40$, some of the operators have a poorer signal and the resulting masses have systematic errors that may exceed the statistical errors in some cases.

The vector meson mass m_ρ is measured using the same procedure as outlined above, but we measure only the local representation $\mathbf{r}^{\sigma_s\sigma_{123}} = \mathbf{3}'' + +$. The fitting ranges that we use for m_ρ match those used for the pions.

IV. RESULTS

A. Flavor symmetry breaking

Our data in Tables III-VII show that the π spectrum for each fermion action falls into the same general pattern shown by previous studies [5]. The state corresponding to the Goldstone pion ($r^{\sigma_s\sigma_{123}} = 1 + -$) is clearly lighter than the other pions. We also expect the splittings to be $O(a^2)$, and indeed the mass differences are smallest for the finest lattice ($\beta = 8.00$) and largest for the coarsest lattice ($\beta = 7.40$). Because we use a Symanzik-improved gauge action, the mass splittings for all actions are also reduced compared to unimproved gauge actions [12].

In general, we expect the different representations to yield different masses. However some of the representations are degenerate at $O(a^2)$, differing only at $O(a^4)$ [13]. In particular, we expect the following pairs of representations to be nearly degenerate: $1 + +$ and $3'' - -$, $3'' - +$ and $3'' + -$, and $3'' + +$ and $1 - -$. This approximate degeneracy is evident for each of the fermion actions. Our precision is not enough to discern the expected pattern of $O(a^4)$ splittings.

Using the data collected in Tables III-VII, we extrapolate each of the 15 different pions to the chiral limit ($m_q \rightarrow 0$). These fits were done using the expected chiral form:

$$m_\pi^2(m_q) = m_\pi^2(m_q = 0) + Bm_q \quad (11)$$

Figure 1 shows the result of a typical chiral fit for each of the 7 distinct representations. Tables VIII-X give the full result of these extrapolations. In the continuum limit, we expect the Goldstone pion to have vanishing mass as $m_q \rightarrow 0$. In our case, m_π does not vanish at $m_q = 0$ due to finite volume effects.

Figures 2-4 show the chiral extrapolated values of m_π for the different fermion actions. The flavor symmetry breaking, characterized by the mass of the non-Goldstone pions, is worst for naive staggered fermions of all the actions tested. The p4fat3 action, which uses three-link smearing, is a significant improvement over the naive staggered action. However, the three highly-improved actions (Asqtad, p4fat7, p4fat7tad) show the best flavor-symmetry characteristics. These three actions give similar results. For $\beta = 7.40$, p4fat7 and Asqtad agree to within statistical errors, while p4fat7tad is slightly better. For $\beta = 7.75$ and $\beta = 8.00$, the p4 actions are slightly better than Asqtad, and tadpole improvement seems to have little effect - p4fat7 and p4fat7tad agree to within errors. Figure 5 shows the mass

splitting as a function of a^2 . As expected, the quantity $m_\pi^2 - m_G^2$ vanishes linearly with a^2 for each of the actions tested.

B. m_ρ vs. r_1 scaling

We also measured the vector meson mass m_ρ for several different values of m_q . Table XI gives m_ρ extrapolated to the $m_q \rightarrow 0$ limit using the linear chiral form:

$$m_\rho(m_q) = m_\rho(m_q = 0) + Bm_q \quad (12)$$

We wish to compare the scale determined by m_ρ with the parameter r_1 extracted from the static quark potential. The values for r_1 that we use are calculated by the MILC collaboration on these lattices and are used in Ref. [9] to check the scaling of the Asqtad action. $r_1/a = 1.44(1), 2.08(5), 2.653(10)$ for $\beta = 7.40, 7.75, 8.00$ respectively.

Figure 6 shows $m_\rho r_1$ plotted against the lattice spacing $(a/r_1)^2$. For Asqtad and p4fat3 actions, $m_\rho r_1$ does not change appreciably over this range. For p4fat7 and p4fat7tad, we seem to see a 10% decrease in $m_\rho r_1$ from the finest lattice to the coarsest lattice.

V. CONCLUSIONS

We have made a detailed comparison of the various different variants of improved staggered actions as they relate to flavor symmetry breaking in the π spectrum and the scaling of the ρ mass.

As expected, the flavor symmetry violations are most severe for the coarsest lattices. All four variants of improved staggered fermions (Asqtad, p4fat3, p4fat7, p4fat7tad) exhibit much better flavor symmetry properties than naive staggered fermions. It seems that gauge-link fattening is the most important factor in these improvements. While the p4fat3 action is better than normal staggered, it is noticeably worse than the more highly improved actions. Among the three actions which employ the most smearing (Asqtad, p4fat7, p4fat7tad), it seems like the p4 variants are very slightly preferred to Asqtad. Also, tadpole improvement seems to have very little affect on the pattern of flavor symmetry breaking.

As for m_ρ , we find that all the improved actions show only mild deviations from scaling in the set of ensembles that we have examined. All of them perform better than naive staggered, although p4fat7 and p4fat7tad show a 10% variation in $m_\rho r_1$.

REFERENCES

- [1] S. Naik, Nucl. Phys. **B316**, 238 (1989).
- [2] U. M. Heller, F. Karsch, and B. Sturm, Phys. Rev. **D60**, 114502 (1999), hep-lat/9901010.
- [3] K. Orginos, D. Toussaint, and R. L. Sugar (MILC), Phys. Rev. **D60**, 054503 (1999), hep-lat/9903032.
- [4] T. Blum *et al.*, Phys. Rev. **D55**, 1133 (1997), hep-lat/9609036.
- [5] N. Ishizuka, M. Fukugita, H. Mino, M. Okawa, and A. Ukawa, Nucl. Phys. **B411**, 875 (1994).
- [6] C. Aubin *et al.*, Phys. Rev. **D70**, 094505 (2004), hep-lat/0402030.
- [7] F. Karsch, E. Laermann, and A. Peikert, Phys. Lett. **B478**, 447 (2000), hep-lat/0002003.
- [8] C. Bernard *et al.* (MILC), Phys. Rev. **D71**, 034504 (2005), hep-lat/0405029.
- [9] C. W. Bernard *et al.* (MILC), Phys. Rev. **D61**, 111502 (2000), hep-lat/9912018.
- [10] M. F. L. Golterman, Nucl. Phys. **B273**, 663 (1986).
- [11] F. Karsch, E. Laermann, and A. Peikert, Nucl. Phys. **B605**, 579 (2001), hep-lat/0012023.
- [12] T. A. DeGrand, A. Hasenfratz, and T. G. Kovacs, Phys. Rev. **D67**, 054501 (2003), hep-lat/0211006.
- [13] W.-J. Lee and S. R. Sharpe, Phys. Rev. **D60**, 114503 (1999), hep-lat/9905023.

ACKNOWLEDGMENTS

We thank RIKEN, Brookhaven National Laboratory and the U.S. Department of Energy for providing the facilities essential for the completion of this work.

The numerical computations were done on the QCDOC computers, located at Columbia University and Brookhaven National Lab.

TABLES

Action	c_1	c_{Naik}	c_{knight}	c_3	c_5	c_7	c_{Lepage}
Asqtad	$1/8 + 3/8 + 1/8$	$-1/24u_0^2$	0	$1/16u_0^2$	$1/64u_0^4$	$1/384u_0^6$	$-1/16u_0^4$
p4fat3	15/44	0	1/24	3/44	0	0	0
p4fat7	$1/8 - 1/4$	0	1/24	1/16	1/64	1/384	0
p4fat7tad	$1/8 - 1/4$	0	$1/24u_0^2$	$1/16u_0^2$	$1/64u_0^4$	$1/384u_0^6$	0
staggered	1	0	0	0	0	0	0

TABLE I. Parameters for the different fermion actions. u_0 is the tadpole-improvement coefficient, $u_0 = \langle \square \rangle^{1/4}$

$r^{\sigma_s \sigma_{123}}$	$\phi(\vec{A})$	δ
1 + +	1	0
1 + -	$\eta_4 \zeta_4$	0
3'' - -	$\zeta_k \epsilon$	$\hat{\mathbf{k}}$
3'' - +	$\eta_4 \zeta_4 \zeta_k \epsilon$	$\hat{\mathbf{k}}$
3'' + +	$\zeta_k \zeta_l \epsilon_{klm}$	$\hat{\mathbf{k}} + \hat{\mathbf{l}}$
3'' + -	$\eta_4 \zeta_4 \zeta_k \zeta_l \epsilon_{klm}$	$\hat{\mathbf{k}} + \hat{\mathbf{l}}$
1 - -	$\eta_4 \zeta_4 \eta_1 \eta_2 \eta_3$	$\hat{\mathbf{1}} + \hat{\mathbf{2}} + \hat{\mathbf{3}}$

TABLE II. Staggered Pions. $\eta_\mu = (-1)^{A_1 + \dots + A_{\mu-1}}$, $\zeta_\mu = (-1)^{A_{\mu+1} + \dots + A_4}$, $\epsilon = (-1)^{A_1 + \dots + A_4}$, $\hat{\mathbf{k}} \neq \hat{\mathbf{l}}$

$r^{\sigma_s \sigma_{123}}$	$\beta = 7.40$			$\beta = 7.75$			$\beta = 8.00$		
	$m_q a =$.02	.03	.04	.02	.03	.04	.01	.02
1 + -	0.3605(3)	0.4390(3)	0.5047(3)	0.314(1)	0.383(1)	0.440(1)	0.2003(5)	0.2800(5)	0.3409(5)
1 + +	0.644(8)	0.690(4)	0.734(3)	0.399(2)	0.455(2)	0.504(1)	0.247(1)	0.3145(10)	0.3693(8)
3'' - -	0.648(2)	0.698(1)	0.7444(9)	0.401(2)	0.457(1)	0.506(1)	0.2474(7)	0.3142(7)	0.3689(6)
3'' - +	0.78(1)	0.824(6)	0.863(5)	0.455(3)	0.504(2)	0.548(2)	0.278(2)	0.338(1)	0.3883(10)
3'' + +	0.90(2)	0.93(1)	0.96(1)	0.502(4)	0.543(3)	0.582(3)	0.303(2)	0.358(2)	0.405(1)
3'' + -	0.802(3)	0.840(2)	0.877(2)	0.456(2)	0.504(1)	0.549(1)	0.2791(8)	0.3379(7)	0.3882(7)
1 - -	0.90(1)	0.935(8)	0.968(6)	0.498(3)	0.541(2)	0.582(2)	0.306(1)	0.3585(8)	0.4049(8)

TABLE III. Asqtad pion masses

$\mathbf{r}^{\sigma_s\sigma_{123}}$	$\beta = 7.40$			$\beta = 7.75$			$\beta = 8.00$		
	$m_q a =$.02	.03	.04	.02	.03	.04	.01	.02
1 + -	0.3136(2)	0.4395(2)	0.5346(2)	0.2781(6)	0.3893(9)	0.474(1)	0.2469(4)	0.3459(5)	0.4218(5)
1 + +	0.75(3)	0.80(1)	0.861(6)	0.416(3)	0.503(2)	0.576(2)	0.310(2)	0.395(1)	0.4650(8)
3'' - -	0.721(3)	0.792(1)	0.857(1)	0.420(1)	0.504(1)	0.576(1)	0.3094(7)	0.3941(6)	0.4638(6)
3'' - +	0.94(4)	0.96(2)	1.012(10)	0.495(4)	0.569(3)	0.634(2)	0.348(2)	0.425(1)	0.4905(10)
3'' + +	1.05(8)	1.11(4)	1.14(2)	0.549(6)	0.614(4)	0.673(3)	0.378(3)	0.448(1)	0.510(1)
3'' + -	0.904(8)	0.966(3)	1.023(3)	0.495(2)	0.568(2)	0.633(2)	0.3481(8)	0.4244(7)	0.4898(7)
1 - -	1.00(3)	1.05(1)	1.112(9)	0.548(4)	0.612(2)	0.672(2)	0.378(1)	0.4477(9)	0.5093(8)

TABLE IV. p4fat3 pion masses

$\mathbf{r}^{\sigma_s\sigma_{123}}$	$\beta = 7.40$			$\beta = 7.75$			$\beta = 8.00$		
	$m_q a =$.02	.03	.04	.02	.03	.04	.01	.02
1 + -	0.4205(3)	0.5832(3)	0.7035(3)	0.3216(8)	0.449(1)	0.5467(9)	0.2727(6)	0.3812(6)	0.4651(6)
1 + +	0.681(6)	0.798(3)	0.896(2)	0.395(2)	0.504(2)	0.593(1)	0.302(1)	0.4019(9)	0.4821(7)
3'' - -	0.681(1)	0.8003(9)	0.8999(8)	0.396(2)	0.504(1)	0.593(1)	0.3021(7)	0.4014(7)	0.4815(6)
3'' - +	0.789(6)	0.895(4)	0.982(3)	0.442(3)	0.539(2)	0.621(2)	0.323(2)	0.416(1)	0.4926(7)
3'' + +	0.90(1)	0.978(6)	1.054(4)	0.484(4)	0.569(3)	0.645(2)	0.341(2)	0.428(1)	0.5019(8)
3'' + -	0.801(2)	0.901(2)	0.988(1)	0.443(2)	0.539(1)	0.621(1)	0.3233(8)	0.4156(7)	0.4924(7)
1 - -	0.894(6)	0.980(4)	1.057(2)	0.483(2)	0.569(2)	0.645(2)	0.3424(9)	0.4283(8)	0.5019(7)

TABLE V. p4fat7 pion masses

$\mathbf{r}^{\sigma_s\sigma_{123}}$	$\beta = 7.40$			$\beta = 7.75$			$\beta = 8.00$		
	$m_q a =$.02	.03	.04	.02	.03	.04	.01	.02
1 + -	0.4227(3)	0.5139(3)	0.5900(3)	0.449(1)	0.5467(9)	0.6293(9)	0.2161(6)	0.3015(6)	0.3669(6)
1 + +	0.643(4)	0.708(3)	0.766(2)	0.504(2)	0.593(1)	0.671(1)	0.250(2)	0.326(1)	0.3870(10)
3'' - -	0.6476(10)	0.7124(9)	0.7708(8)	0.504(1)	0.593(1)	0.670(1)	0.2518(9)	0.3263(7)	0.3866(7)
3'' - +	0.762(5)	0.816(4)	0.867(3)	0.539(2)	0.621(2)	0.695(1)	0.276(2)	0.345(2)	0.402(1)
3'' + +	0.873(10)	0.915(6)	0.956(5)	0.569(3)	0.645(2)	0.715(2)	0.300(3)	0.361(2)	0.414(1)
3'' + -	0.775(2)	0.828(2)	0.877(1)	0.539(1)	0.621(1)	0.695(1)	0.279(1)	0.3452(8)	0.4014(7)
1 - -	0.869(7)	0.915(4)	0.957(3)	0.569(2)	0.645(2)	0.715(1)	0.302(1)	0.3622(8)	0.4147(8)

TABLE VI. p4fat7tad pion masses

$\mathbf{r}^{\sigma_s \sigma_{123}}$	$\beta = 7.40$				$\beta = 7.75$			
	$m_q a =$.01	.02	.03	.04	.01	.02	.03
1 + -	0.2738(2)	0.3834(2)	0.4655(2)	0.5332(2)	0.2769(4)	0.3861(4)	0.4676(4)	0.5351(4)
1 + +	0.93(4)	0.98(2)	1.02(1)	1.063(10)	0.540(8)	0.617(4)	0.687(3)	0.749(2)
3'' - -	0.941(5)	0.997(4)	1.045(3)	1.090(2)	0.539(2)	0.620(2)	0.689(1)	0.750(1)
3'' - +	1.2(1)	1.23(3)	1.26(3)	1.29(2)	0.631(8)	0.698(5)	0.762(4)	0.820(3)
3'' + +	1.18(6)	1.25(3)	1.31(2)	1.36(2)	0.67(1)	0.731(6)	0.793(5)	0.849(4)
3'' + -	1.13(1)	1.171(7)	1.218(5)	1.264(4)	0.618(4)	0.690(2)	0.755(2)	0.815(2)
1 - -	1.16(3)	1.25(2)	1.31(1)	1.36(1)	0.664(7)	0.732(4)	0.795(3)	0.851(3)
Type	$\beta = 8.00$							
$m_q a =$.01	.02	.03					
1 + -	0.2580(3)	0.3604(3)	0.4379(3)					
1 + +	0.381(2)	0.467(1)	0.5393(8)					
3'' - -	0.3805(7)	0.4660(6)	0.5379(6)					
3'' - +	0.425(2)	0.502(1)	0.572(1)					
3'' + +	0.449(3)	0.523(2)	0.590(1)					
3'' + -	0.4215(10)	0.5008(8)	0.5698(7)					
1 - -	0.447(1)	0.523(1)	0.5889(9)					

TABLE VII. Naive staggered pion masses

$\mathbf{r}^{\sigma_s \sigma_{123}}$	Asqtad	p4fat3	p4fat7	p4fat7tad	Staggered
1 + -	0.072(1)	0.0675(7)	0.1317(9)	0.096(1)	0.0723(4)
1 + +	0.54(1)	0.68(3)	0.545(9)	0.490(9)	0.88(4)
3'' - -	0.534(3)	0.642(3)	0.540(2)	0.49(2)	0.890(6)
3'' - +	0.69(2)	0.88(3)	0.677(9)	0.639(8)	1.18(6)
3'' + +	0.84(3)	1.02(10)	0.81(2)	0.78(2)	1.13(5)
3'' + -	0.719(6)	0.841(10)	0.691(4)	0.658(3)	1.07(1)
1 - -	0.83(2)	0.93(3)	0.802(9)	0.77(1)	1.11(3)

TABLE VIII. m_π extrapolated to $m_q = 0$ for $\beta = 7.40$.

$\mathbf{r}^{\sigma_s \sigma_{123}}$	Asqtad	p4fat3	p4fat7	p4fat7tad	Staggered
1 + -	0.064(3)	0.061(2)	0.075(3)	0.086(4)	0.08(1)
1 + +	0.253(4)	0.307(5)	0.240(4)	0.239(3)	0.449(9)
3'' - -	0.257(2)	0.314(2)	0.244(2)	0.243(2)	0.449(2)
3'' - +	0.339(5)	0.408(6)	0.317(4)	0.314(4)	0.552(9)
3'' + +	0.407(7)	0.474(9)	0.377(5)	0.370(5)	0.59(1)
3'' + -	0.338(3)	0.409(3)	0.319(2)	0.315(3)	0.537(5)
1 - -	0.397(4)	0.473(6)	0.377(3)	0.370(3)	0.590(8)

TABLE IX. m_π extrapolated to $m_q = 0$ for $\beta = 7.75$.

$\mathbf{r}^{\sigma_s \sigma_{123}}$	Asqtad	p4fat3	p4fat7	p4fat7tad	Staggered
1 + -	0.046(2)	0.050(2)	0.058(3)	0.052(2)	0.063(1)
1 + +	0.152(3)	0.191(3)	0.142(3)	0.138(4)	0.268(4)
3'' - -	0.154(1)	0.190(1)	0.145(1)	0.143(1)	0.269(1)
3'' - +	0.201(3)	0.248(3)	0.186(3)	0.185(3)	0.326(4)
3'' + +	0.237(4)	0.290(4)	0.219(3)	0.222(4)	0.357(5)
3'' + -	0.204(1)	0.248(1)	0.188(1)	0.189(1)	0.323(2)
1 - -	0.242(2)	0.290(2)	0.223(1)	0.226(2)	0.356(2)

TABLE X. m_π extrapolated to $m_q = 0$ for $\beta = 8.00$.

Action	$\beta = 7.40$	$\beta = 7.75$	$\beta = 8.00$
Staggered	1.18(2)	0.76(3)	0.628(9)
Asqtad	1.09(6)	0.73(3)	0.602(13)
p4fat3	1.09(8)	0.75(3)	0.596(9)
p4fat7	0.99(3)	0.73(3)	0.586(6)
p4fat7tad	1.00(4)	0.73(2)	0.585(11)

TABLE XI. m_ρ extrapolated to $m_q \rightarrow 0$ for the different actions

FIGURES

Chiral extrapolation for m_π

$16^3 \times 32$, p4fat3, $\beta=7.40$

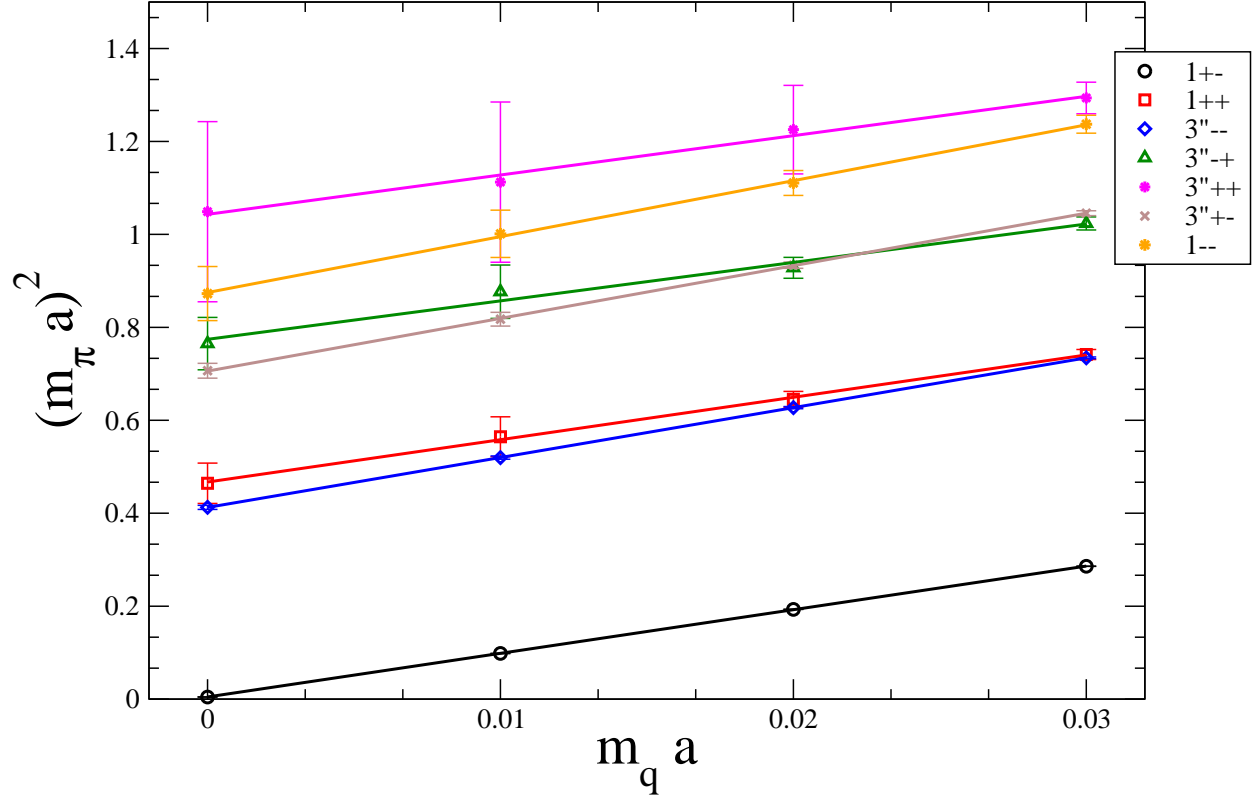


FIG. 1. Chiral extrapolation of m_π^2 for p4fat3 action, $\beta = 7.40$

Chiral extrapolated m_π
 $16^3 \times 32, \beta=7.40$

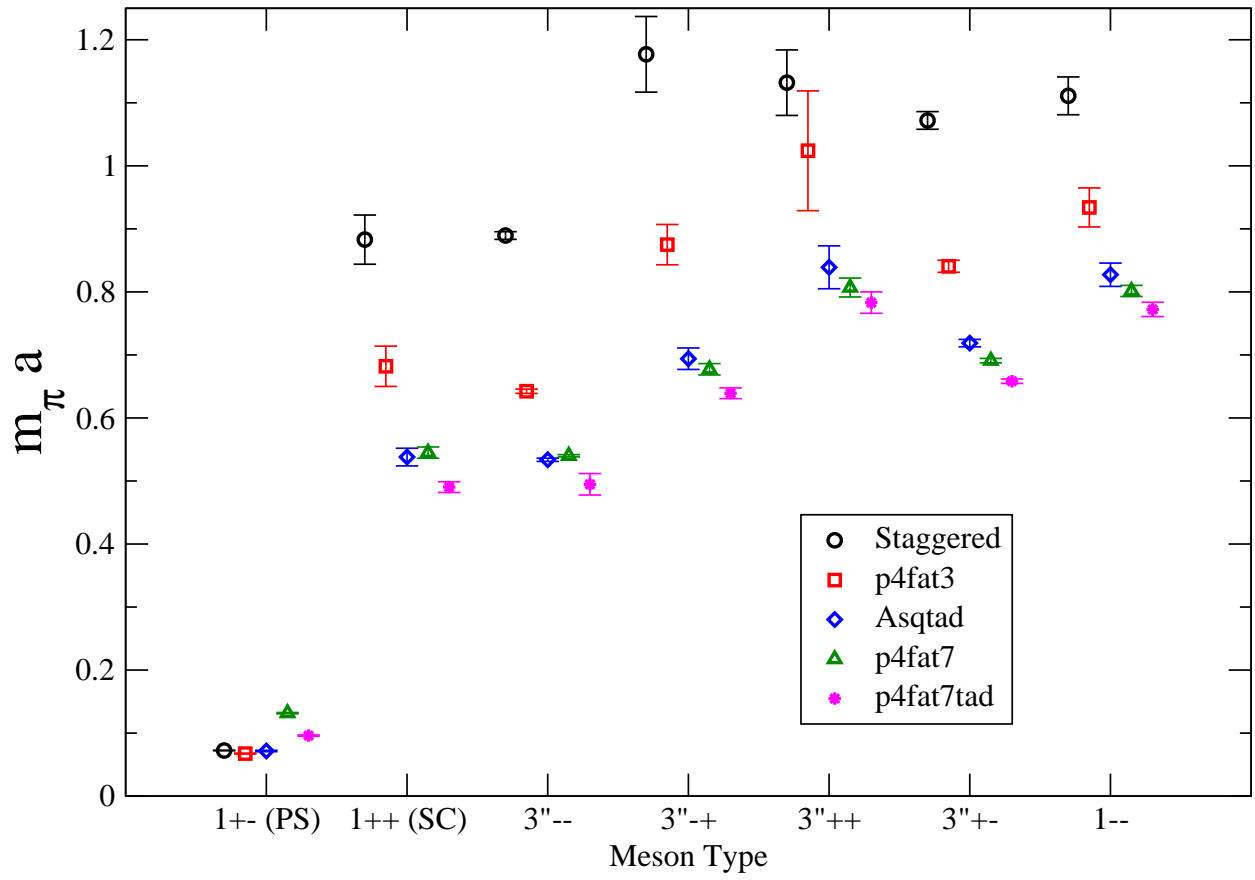


FIG. 2. Flavor symmetry breaking of m_π in the chiral limit for $\beta = 7.40$.

Chiral extrapolated m_π
 $16^3 \times 32, \beta=7.75$

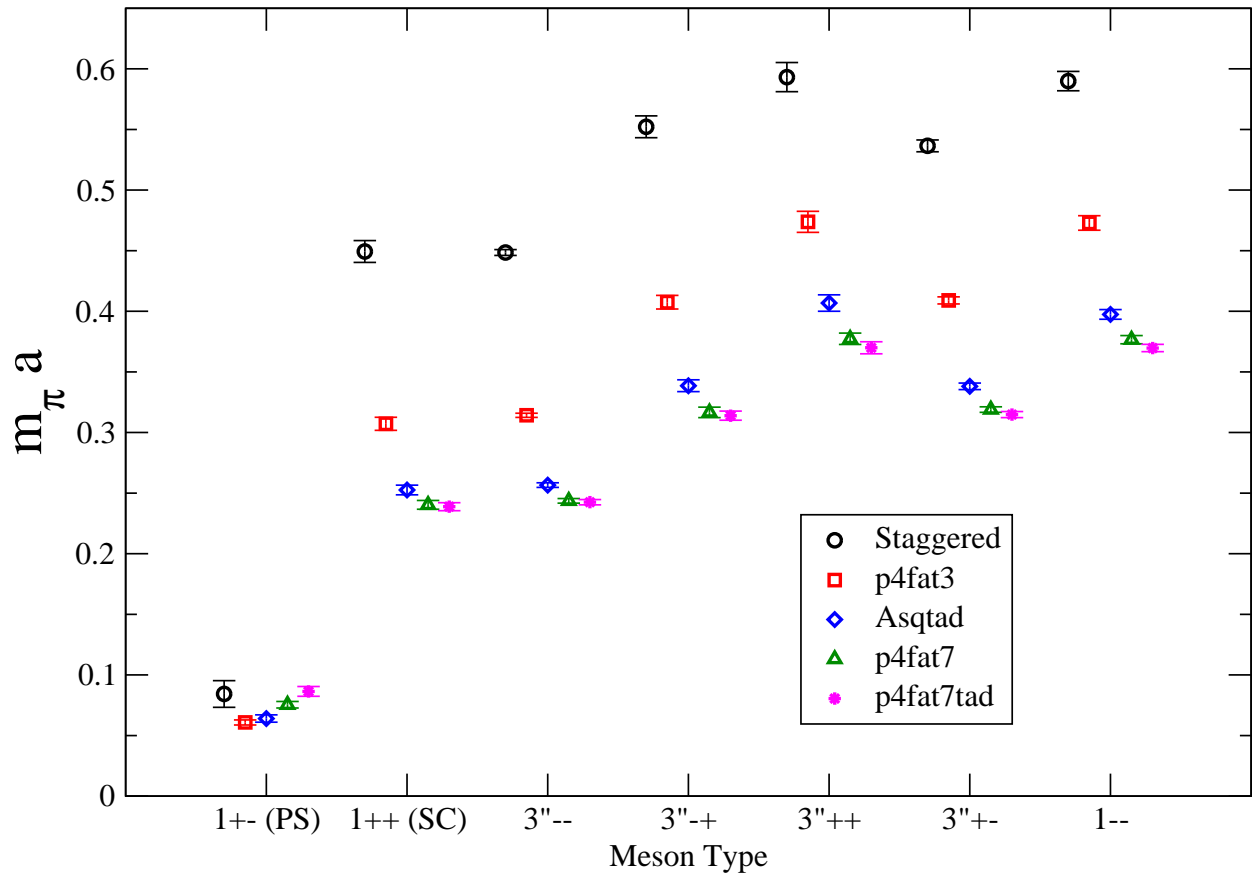


FIG. 3. Flavor symmetry breaking of m_π in the chiral limit for $\beta = 7.75$.

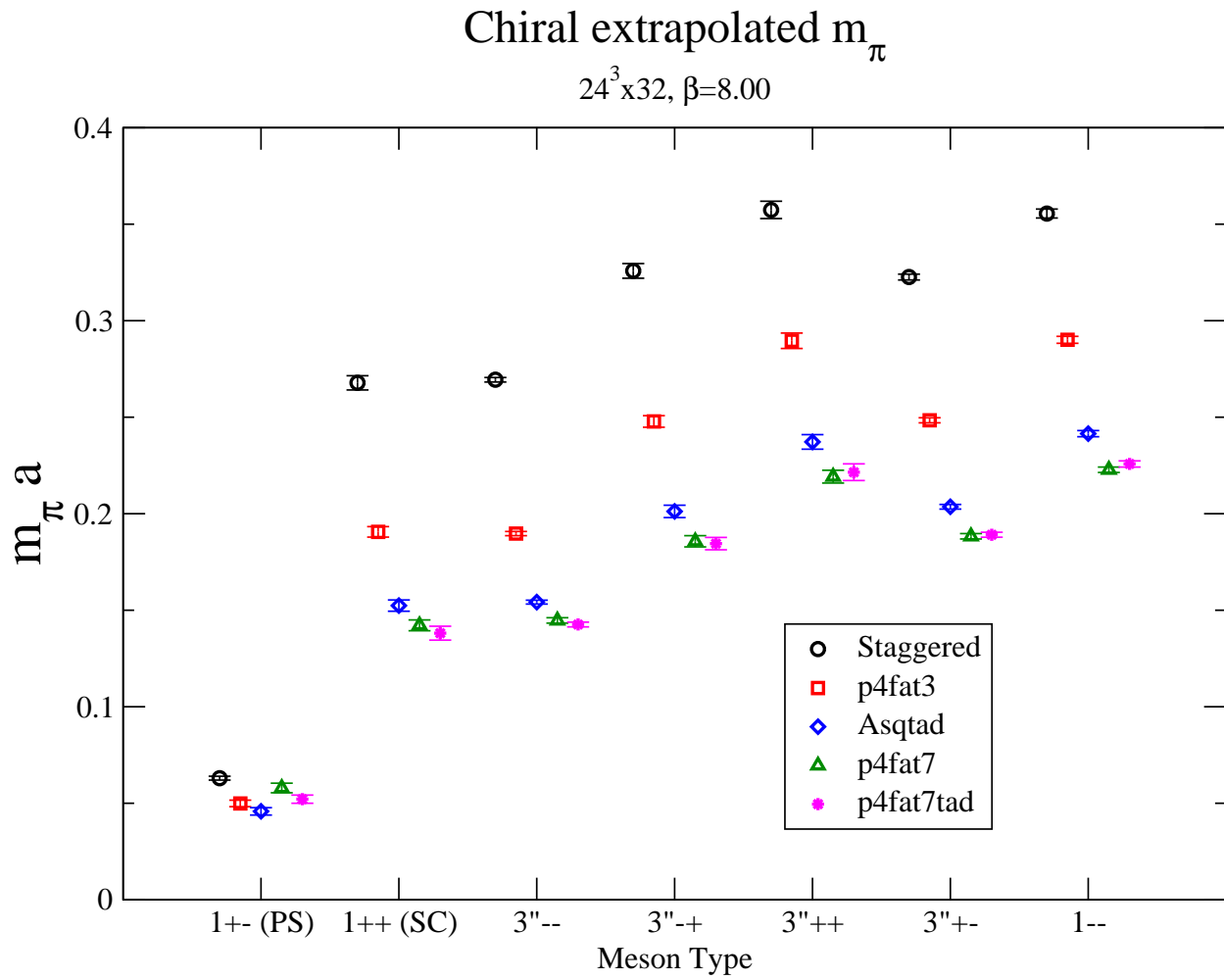


FIG. 4. Flavor symmetry breaking of m_π in the chiral limit for $\beta = 8.00$.

Pion mass splitting

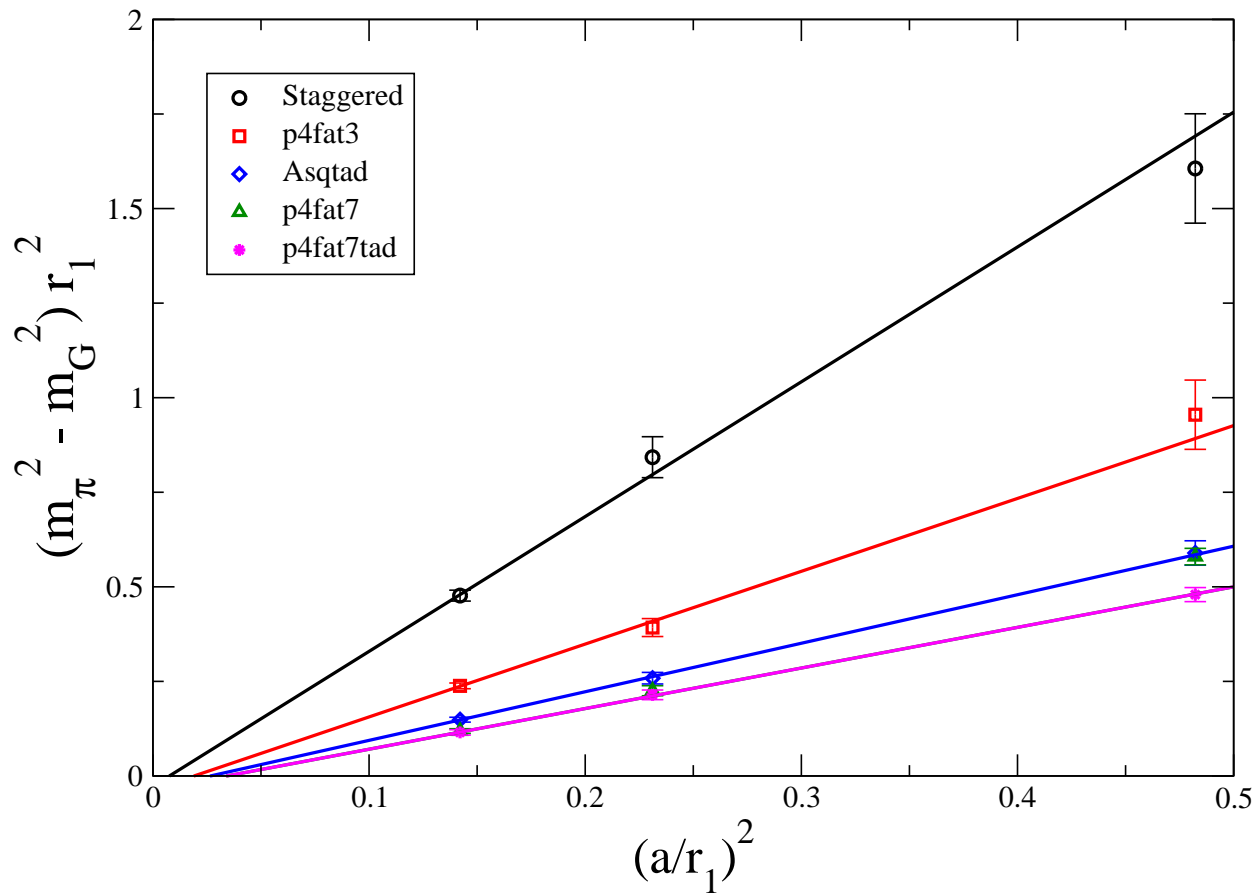


FIG. 5. Pion mass splittings for chirally extrapolated values of m_π . m_π corresponds to $r^{\sigma_s \sigma_{123}} = 1++$ while m_G is the mass of the Goldstone pion.

$m_\rho r_1$ vs. $(a / r_1)^2$

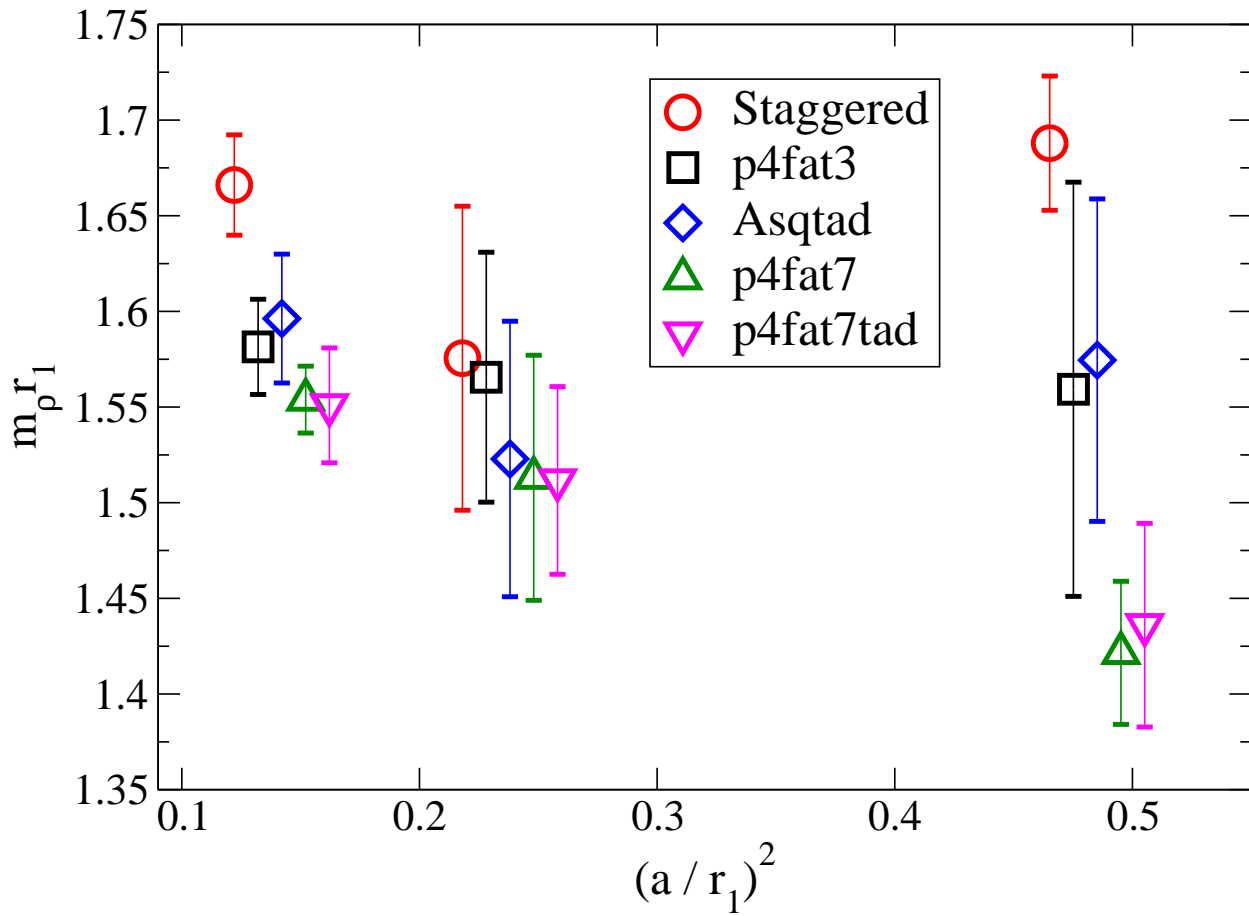


FIG. 6. Scaling of $m_\rho r_1$ vs. $(a/r_1)^2$ for various actions (points offset for clarity)